Rotor Winding Unbalance Fault Detection in Induction Motors Using Stray Flux and the Teager–Kaiser Energy Operator

Hassan Shakeri, Mohammad Hoseintabar Marzebali, Vahid Abolghasemi, and Saeed Hajnayeb

Abstract: **Stray flux signals play a key role in fault detection and identification in induction motors. In this study, the frequency spectrum of the stray flux is analyzed under various operating conditions of a wound-rotor induction motor with a rotor asymmetry fault (RAF). The results show that at high speeds, the fault indicators are affected by energy leakage from the fundamental frequency. This leakage introduces noise related to the fundamental frequency and prevents reliable variations correlated with fault severity. To mitigate this effect, the Teager--Kaiser energy operator (TKEO) is employed to suppress the energy leakage associated with the supply frequency.**

Keywords: **Rotor fault, stray flux, fault indicators, condition monitoring, spectral analysis.**

I Introduction

Electric motors are widely used in numerous industrial processes, including air purification systems, food and textile production, transportation, and mining industries. Among the various types of electric motors, induction motors are the most widely employed because of their low cost, simple structure, and high reliability. Induction motors are classified into two main types based on their rotor configuration: wound-rotor and squirrel-cage motors. The wound-rotor type is particularly suitable for applications requiring high starting torque, such as conveyors and compressors, whereas the squirrel-cage type is commonly used in applications that require constant speed and automatic starting capability. Despite their advantages, induction motors are exposed to various types of faults, including rotor faults (e.g., rotor winding faults or broken bars), stator winding faults (such as short circuits), and bearing defects [1, 2]. In the IEEE and EPRI technical reports [3], rotor faults in induction motors account for about 10% of all failures, mainly due to thermal stresses from overloads and frequent starts, as well as electromagnetic, mechanical, and dynamic stresses. This statistic is important because rotor unbalance, a common consequence of these stresses, causes an unbalanced magnetic force in the motor air gap. This unsymmetrical force, in turn, unbalances the line currents, increases torque pulsation, and exacerbates power losses, all of which lead to a significant reduction in efficiency, increased heat generation, and additional thermal stresses. Ultimately, this chain of deterioration not only severely reduces the useful life of the motor but also causes sudden and unplanned shutdowns in the production process, resulting in significant financial losses from production stoppages, emergency repairs, and equipment replacement; therefore, continuous monitoring of rotor condition and timely detection of unbalance play a vital role in increasing system reliability and reducing operating costs [4, 5].

Various signals, including temperature, vibration, current, and magnetic flux, have been introduced for fault detection in induction motors. By processing these signals, different types of faults in induction motors can be identified. Each signal, despite its advantages, also presents certain limitations [6]. In [7], a simple and portable fault detection device based on temperature signals is proposed. In [8], vibration and acoustic signal analysis is employed for the detection of mechanical faults such as broken rotor bars and bearing defects. Stray flux signal analysis (SFSA) has demonstrated that, unlike the motor current signature analysis (MCSA) method, it is not significantly affected by load fluctuations.

Previous studies have shown that when rotor bars are symmetrically broken, no asymmetry appears in the stator current, rendering MCSA incapable of detecting the fault. In contrast, SFSA does not depend on the position of the broken rotor bars and can therefore overcome the limitations associated with current-based analysis [9]. Moreover, magnetic flux, as a quantity related to the entire electromagnetic structure of the induction motor, provides valuable information about both the mechanical and electrical components of the machine. In comparison, some other diagnostic signals are sensitive only to specific parts of the motor. Additional advantages of flux-based analysis include the relatively low cost of implementing certain flux sensors and the high capability of this approach for

Manuscript received 21 September, 2026; revised 6 October, 2026; accepted 25 October, 2026.

H. Shakeri is with the faculty of electrical engineering, Shahrood University of Technology, Shahrood 36199-95161, Iran (e-mail: hasanshakrie@gmail.com).

M. Hoseintabar Marzebali is with the faculty of electrical engineering, Shahrood University of Technology, Shahrood 36199-95161, Iran (e-mail: m.hoseintabar@shahroodut.ac.ir).

V. Abolghasemi is with the school of computer science and electronic engineering, University of ESSEX Colchester, UK (e-mail: v.abolghasemi@essex.ac.uk).

S. Hajnayeb is the faculty of electrical engineering, Shahrood University of Technology, Shahrood 36199-95161, Iran (e-mail: saeed.hajnayeb@shahroodut.ac.ir).

Corresponding author: M. Hoseintabar Marzebali.

detecting a wide range of faults [10].

Most stator fault signature analysis methodologies, particularly MCSA, rely on the detection of sideband frequency components located around the fundamental supply frequency. The fast Fourier transform (FFT) remains a widely adopted tool for such analyses; however, its application is predominantly confined to steady-state operating conditions, especially in the detection of unbalanced conditions in wound-rotor induction machines. Several alternative techniques—including the rectified orthogonal axes technique (ROAT), the frequency-domain energy operator (FDEO), the adaptive extended Kalman filter (AEKF), rectified current analysis, and Park's vector approach—have been proposed to extend the applicability of MCSA. Nevertheless, these methods are not comprehensively addressed within the conventional SFSA framework [11, 12]. In [10], the Teager–Kaiser energy operator (TKEO) is introduced as a simple yet effective means of suppressing the dominant supply-frequency component in induction motor current signals, thereby enhancing the visibility of weak fault-induced harmonic components. The method is particularly appealing for real-time deployment owing to its low computational cost and high speed. However, to date, no systematic investigation has been conducted into the performance of the TKEO when applied to stray flux signals.

In this paper, the TKEO is applied to the analysis of the stray flux signal for the detection of rotor imbalance faults. The results demonstrate that at high operating speeds of the induction motor, conventional frequency-spectrum analysis fails to reliably identify fault-related components. By contrast, the proposed method significantly enhances fault detection sensitivity, enabling accurate identification of fault components.

II BASIC THEORY FOR THE STARY FLUX

The stray flux of an induction machine is generally regarded as a residual, non-useful magnetic phenomenon that does not contribute to the electromechanical energy conversion process; that is, it plays no role in generating output torque. In this paper, the term "stray flux" specifically refers to magnetic flux that radiates outside the machine frame, making it accessible for non-invasive measurement and diagnostic purposes.

A Effect of air-gap MMF in the stray flux

In idealized modeling of three-phase induction machines, symmetrical winding distributions and the absence of stray flux components are conventionally assumed under healthy operating conditions. In practice, however, inherent structural asymmetries arising from stator slotting, localized saturation, and non-uniform magnetic properties cause stray flux components to persist in the air gap even under perfectly balanced supply voltages. The frequency spectrum of this stray flux serves as a robust biomarker for condition monitoring of squirrel-cage induction machines. Consequently, any incipient fault—whether inter-turn short circuits in stator windings, bar or end-ring fractures in the rotor cage, or winding defects in wound-rotor machines—alters the spatial harmonic distribution of the air-gap flux density. This perturbation manifests as the emergence of new spectral components or the amplification of existing ones in the current spectra of both the stator and rotor, thereby modifying the baseline spectral signature of the healthy machine.

From a fundamental perspective, the electromotive force induced in both the stator and rotor is critically governed by the discrete winding configuration—including pitch, span, and connection type—as well as by the rotor cage architecture, specifically the number of bars and the manner in which the end rings are interconnected. Hence, any modification in the primary circuit topology—whether due to short circuits, open circuits, or mechanical bar fractures—directly alters the equivalent impedance of the machine, which in turn reshapes the current frequency spectrum. A particularly significant attribute of stray flux from a diagnostic standpoint lies in its inherent dependency on the resultant of stator and rotor currents. This phenomenon renders stray flux a valuable indirect metric for detecting parametric variations in electrical circuits. Accordingly, a search coil mounted on the stator yoke or frame provides a straightforward yet reliable means of simultaneously capturing both supply-frequency harmonics and spatial harmonics originating from the temporal and spatial content of stator and rotor currents. Nevertheless, to quantitatively interpret the frequency spectrum acquired from the search coil signal and to extract fault-specific components, it is necessary to derive the analytical relationships governing the space and time harmonics induced independently by stator and rotor currents.

1 Current harmonics induced in the squirrel cage rotor

For a squirrel-cage three-phase 2-pole induction machine supplied from a three-phase balanced power supply, the developed stator MMF in the air gap can be written as:

$$F_s(t,x) = \frac{3N_sI_s}{\pi}\sum_{\nu=1}^{\infty}\left\{\frac{1}{\nu}\left[\sum_{b=1}^{c}\sin\left(\nu\frac{\tau_{cb}}{\tau_p}\frac{\pi}{2}\right)\right] \times \sin\left(\omega t - \frac{\nu\pi}{\tau_p}x\right)\right\} \tag{1}$$

where ν denotes the stator MMF space harmonic order, I_s denotes the peak value of the stator phase current, ω denotes the angular frequency of the power supply, N_s denotes the number of turns per stator coil, c denotes the number of coils per stator phase, τ_{cb} denotes the pitch of the bth coil, τ_p denotes the pole pitch, and x represents the circumferential position.

The flux induced in the kth mesh of the rotor is as

$$\Phi_{s,r,k}(t) = \int_{x_1}^{x_2}\frac{\mu_0F_s(t,x)}{\delta}\,dx \tag{2}$$

where μ_0 is the air magnetic permeability, l_c is the core length, δ is the air-gap length, and x_1 and x_2 denote the defined positions of the kth mesh.

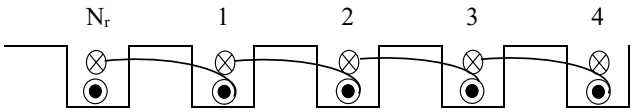


Fig. 1. Equivalent winding of a squirrel-cage rotor winding [13].

The final expression of the flux in (2) is

$$\begin{aligned}\Phi_{sr,k}(t) &= \sum_{\nu=1}^{\infty} \Phi_{\max,\nu} \sin\left\{\left[1 \mp \nu(1-s)\right]\omega t \right. \\ &\qquad \left. \mp \frac{2\nu\pi(k-1)}{pN_r}\right\} \\ \Phi_{\max,\nu} &= \frac{3\mu_0 N_s I_s l_c D_r}{p^2\pi\delta} \sum_{b=1}^{\infty}\left\{\sin\left(\nu\frac{\tau_{cb}}{\tau_p}\frac{\pi}{2}\right)\right. \\ &\qquad \left. \times \sin\left(\nu p\frac{\pi}{N_r}\right)\right\}\end{aligned} \tag{3}$$

where D_r is the external rotor diameter, N_r is the number of rotor meshes, and s is the rotor slip.

From (3), the frequency components induced in the rotor flux by the space harmonics of the stator MMF are given by

$$\begin{aligned} f_{rotor} &= \left[ks - \nu(1-s)\right] f_{supply}, \quad \nu = 6k+1 \\ f_{rotor} &= \left[ks + \nu(1-s)\right] f_{supply}, \quad \nu = 6k-1 \end{aligned} \tag{4}$$

2 Current harmonics induced in the stator windings

A squirrel-cage rotor can be replaced by an equivalent general $2n$-phase, two-layer winding with one slot per pole per phase, as shown in Fig. 1. The pitch of the equivalent winding is equal to one slot. If the squirrel-cage rotor has N_p slots (bars), the rotor structure can be replaced by a winding with N_p phases. The total rotor …

$$\begin{aligned} F_r(t,x) = \sum_{\nu=1}^{\infty} \frac{N_r I_{r\nu\,\max}}{\pi} \sum_{\gamma=1}^{\infty} \frac{1}{\gamma} \sin\left(\frac{\gamma\tau_{cr}}{2}\right) \\ \times \sin(\gamma N_r x \pm s_\nu \omega t) \end{aligned} \tag{5}$$

where $I_{r\nu\,\max}$ is the maximum value of the γth harmonic rotor current and τ_{cr} is the rotor equivalent coil pitch.

The flux induced by the γth harmonics in the bth stator coil is calculated as

$$\begin{aligned}\Phi_{rsb,\gamma}(t) &= \Phi_{\max b,\gamma} \sin\left\{\gamma N_r \frac{\omega_r}{p} t \pm \nu\omega t \right. \\ &\qquad \left. + \gamma\frac{2\pi(b-1)}{3}\right\} \\ \Phi_{\max b,\gamma} &= \frac{\mu_0 I_{r,\nu\,\max} N_r l_c D_r N_s}{\pi\delta\gamma^2} \sin\left(\frac{\gamma\tau_{cr}}{2}\right) \\ &\qquad \times \sin\left(\gamma\frac{\pi}{2}\frac{\tau_{cb}}{\tau_p}\right)\end{aligned} \tag{6}$$

where ω_r is the rotor speed in electrical radians per second.

Then, the frequencies induced by the space harmonics of the rotor MMF in the stator coils can be expressed as

$$f_{stator} = \left[\gamma\frac{N_r}{p}(1-s) \pm \nu\right] f_{supply} \tag{7}$$

The stray flux of a squirrel-cage three-phase induction machine is generated by the coil ends as well as the squirrel-cage rotor end-rings.

$$\Phi_{srav}(t) = k_s i_{s,\omega}(t) + k_i i_{r,b}(t) \tag{8}$$

In the present formulation, the parameters k_s and k_i are distinct proportionality factors that quantify the leakage inductance contributions originating from the coil ends of the stator windings and the end rings of the rotor cage, respectively, while $i_{s,\omega}$ and $i_{r,b}$ denote the corresponding stator winding current and rotor bar current. An external flux sensor, specifically designed to capture the peripheral stray magnetic field, can acquire the signal spectrum of the total stray flux measured at the machine extremities, as expressed in (8). This measured stray flux inherently contains frequency components associated with both the stator and rotor electrical regimes, a characteristic well documented in the literature [13]. This property enables the detection of stator or rotor dissymmetry by analyzing the dominant frequency components.

III TKEO

The TKEO was originally developed for speech signal analysis, where signal amplitudes and phases vary continuously over time. Owing to its ability to track instantaneous energy variations, this operator has subsequently been applied in several fields, including power systems for instantaneous frequency estimation and transient oscillation detection, as well as in the fault diagnosis of electrical machines. One of the key advantages of the TKEO is its ability to capture instantaneous energy-related changes with a very low computational burden, thereby eliminating the need for complex signal processing techniques [14].

A Mathematical definition TKEO

For a continuous signal $x(t)$, the TKEO is calculated as given in (9).

$$\psi(x(t)) = \dot{x}(t)^2 - x(t)\ddot{x}(t) \tag{9}$$

The general formulation of the TKEO for a discrete signal is defined in (10)

$$\psi(x[n]) = x[n]^2 - x[n-1]x[n+1] \tag{10}$$

According to (10), only three consecutive samples are required to compute the instantaneous response of the TKEO. Therefore, this method can be efficiently implemented in DSP processors, as it does not require high storage capacity [14].

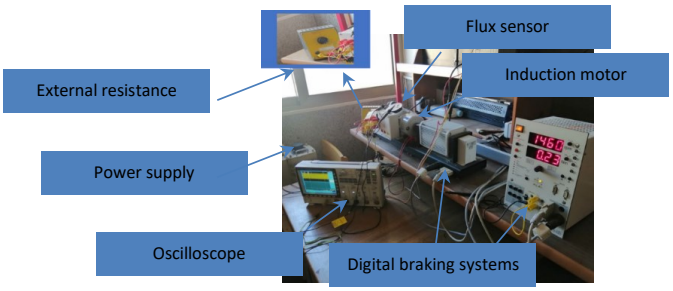


Fig. 2. Laboratory setup for investigating rotor unbalance.

TABLE 1. Specifications of the wound-rotor induction motor.

Parameter	Value
P (W)	270
V (V)	380
f_s (Hz)	50
Pole Pair	2
R_s (Ω)	34.73
R_r (Ω)	32.12
X_{sr} (H)	1.339
X_s (H)	0.139
X_r (H)	0.159
Inertia (kg·m^2)	0.00161

B *Effect of the TKEO on current and flux signals in healthy and faulty conditions*

In this section, the stator current is first analyzed under healthy and faulty conditions. By applying the TKEO, the resulting signal components are identified and examined.

$$i_{healthy}(t) = I_m \cos(\omega t) = I_m \cos(2\pi f t) \tag{11}$$

$$\psi\left(i_{healthy}(t)\right) = I_m^2 \omega^2 \tag{12}$$

$$i_{faulty}(t) = i_{healthy}(t)\left[1 + \beta \cos(\omega_0 t)\right] \tag{13}$$

$$\begin{aligned}\psi\left(i_{faulty}(t)\right) = I_m^2\omega^2 + \frac{1}{2}I_m^2\omega^2\beta\Big(&\cos\left((2\omega^2+\omega_0)t\right)\\ &+\cos\left((2\omega^2-\omega_0)t\right)\Big)\end{aligned} \tag{14}$$

According to (11), the phase current under healthy conditions is assumed to be an ideal sinusoidal waveform, where f_s denotes the supply frequency. Applying the TKEO to the healthy current, $\psi(i_{\text{healthy}}(t))$, yields a constant value, as shown in (12), which represents the envelope of the current signal. In the presence of periodic disturbances, such as broken rotor bars, rotor unbalance, or bearing defects, the fault severity factor β, associated with a characteristic frequency f_0, modulates the motor current. This condition is expressed in (13), where $\omega_0 = 2\pi f_0$. Since the fault-related components are significantly smaller than the fundamental current component, it is assumed that $\beta \ll 1$. Consequently, these components appear as sideband frequencies around the fundamental frequency. Applying the TKEO to the fault-affected current, $\psi(i_{\text{faulty}}(t))$, and neglecting higher-order terms yields expression (14). This expression consists of three components: the first term is a constant component related to the fundamental harmonic of the supply current; the second term oscillates at the fault characteristic frequency; and the third term contains two sideband components located near twice the fundamental frequency.

IV Results

A *Overview of the laboratory test system structure*

The aim of this study is to detect rotor winding unbalance using a stray flux sensor. As illustrated in Fig. 2, an external resistor is connected to the rotor circuit to introduce unbalance. The voltages induced in the sensor winding are recorded using an oscilloscope. The specification of the induction motor tested in this paper is given in Table 1. A digital braking system is employed to control the speed of the induction motor by applying adjustable torque.

B *Sensor characterization*

Among the three primary sensor types employed for measuring external magnetic fields in rotating machines—namely, Hall-effect, magnetoresistive, and search-coil sensors—the search-coil type is preferred in diagnostic applications that require low-frequency spectral analysis. Consequently, this paper employs search-coil sensors; to ensure optimal measurement performance, several critical parameters must be carefully considered during the selection process [15, 16].

- The sensor's physical dimensions, which must be commensurate with the machine scale to ensure adequate spatial resolution;
- The number of turns, which should be tailored to compensate for the attenuation imposed by the stator magnetic circuit and the external machine frame.

Accordingly, this study employs two search-coil sensors, each comprising 6000 turns, with the following electrical specifications: the upper sensor has a resistance of 6 MΩ and an inductance of 620 mH, while the side sensor has a resistance of 6 MΩ and an inductance of 700 mH. The geometric dimensions of both sensors are illustrated in Fig. 3, and their respective mounting positions are shown in Fig. 4.

C *Experimental results*

Rotor unbalance leads to an asymmetric distribution of rotor currents. This asymmetry generates a backward-rotating magnetic field component that rotates in the direction opposite to that of the main field. The frequency of this backward field component is $-sf_s$. Furthermore, the unbalanced rotor field causes fluctuations in the electromagnetic torque. Since the rotor experiences this asymmetry twice during each stator field cycle, the resulting torque ripple frequency is $2sf_s$. This torque ripple affects both the rotor speed and the magnetic flux, thereby generating, in the current and flux signals, the frequency components

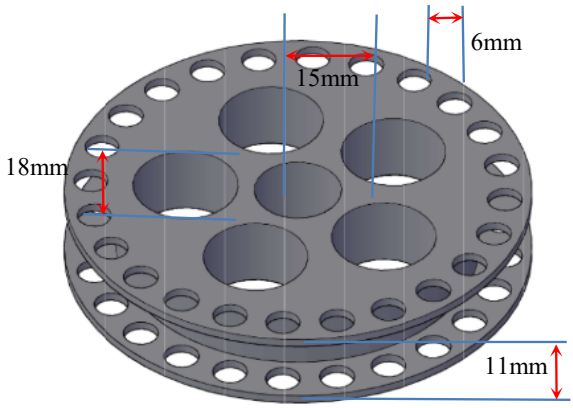


Fig. 3. Dimensions of the sensor coil.

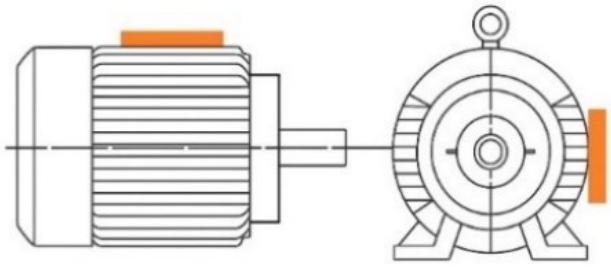


Fig. 4. Sensors position.

described in (15).

$$(1 \pm 2s) f_s \tag{15}$$

The rotor rotates at its mechanical speed, which can be expressed as the mechanical frequency f_r. The currents induced in the rotor bars produce a magnetic field that rotates synchronously with the rotor in space. Consequently, the rotor magnetic field also rotates at the mechanical frequency [17, 18]. As illustrated in Figs. 5–7 and Table 2, the indices corresponding to the frequency components $f_s \pm f_r$ do not exhibit sufficient sensitivity to rotor faults, since their amplitudes do not show a consistent increasing trend with rising fault severity. This observation is consistent with findings reported in [19], which indicate that these components are more strongly influenced by eccentricity and magnetic anisotropy than by rotor asymmetries. In contrast, the indices associated with $f_s - 2sf_s$ display markedly higher sensitivity to rotor faults across all operating speeds, with amplitudes that increase in proportion to fault severity, making them more reliable indicators for rotor fault diagnosis.

D Investigation of the TKEO applied to stray flux

Although conventional FFT-based spectral analysis is capable of detecting fault-related harmonic components over the entire speed range, it requires simultaneous monitoring of multiple indicators, some of which are adversely affected by magnetic anisotropy and eccentricity effects, thereby compromising their diagnostic reliability and complicating the fault interpretation process. In contrast, demodulation techniques—such as TKEO, ROAT, and FDEO—effectively separate fault-related information. Furthermore, as evidenced by the computational complex-

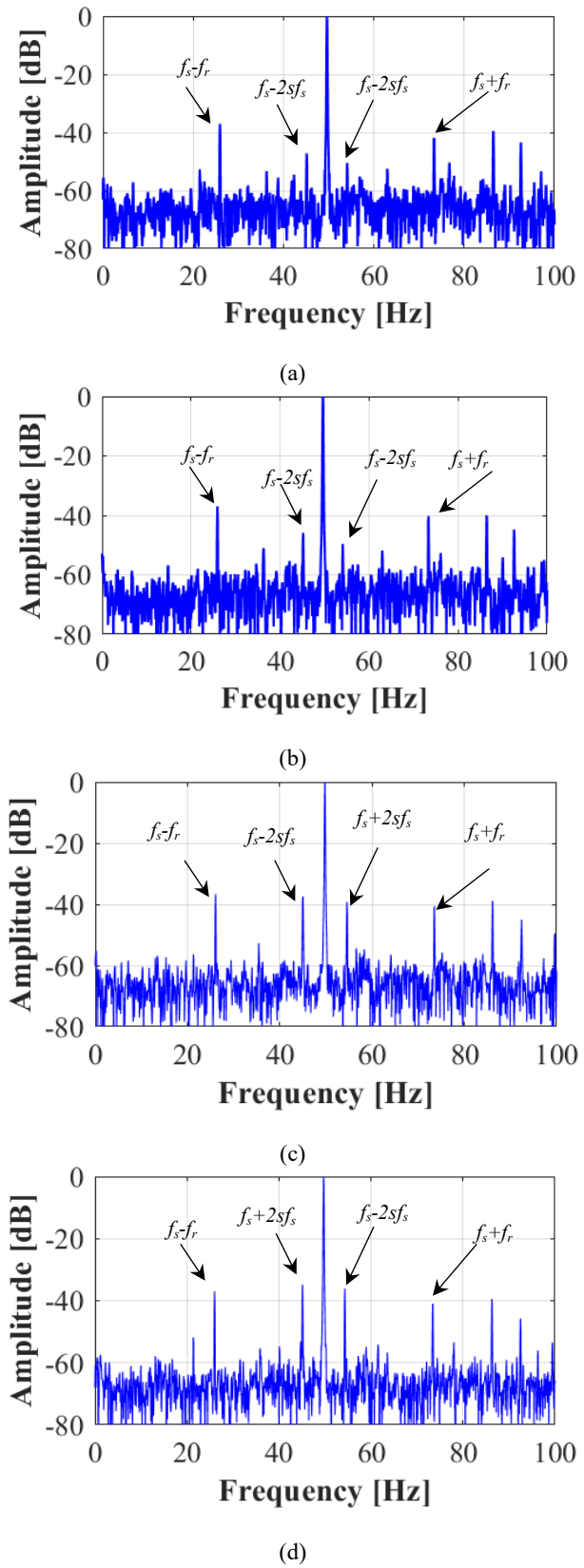


Fig. 5. FFT of the coil sensor at 1420 rpm a) Healthy b) One ohm c) 3 ohms d) 5 ohms.

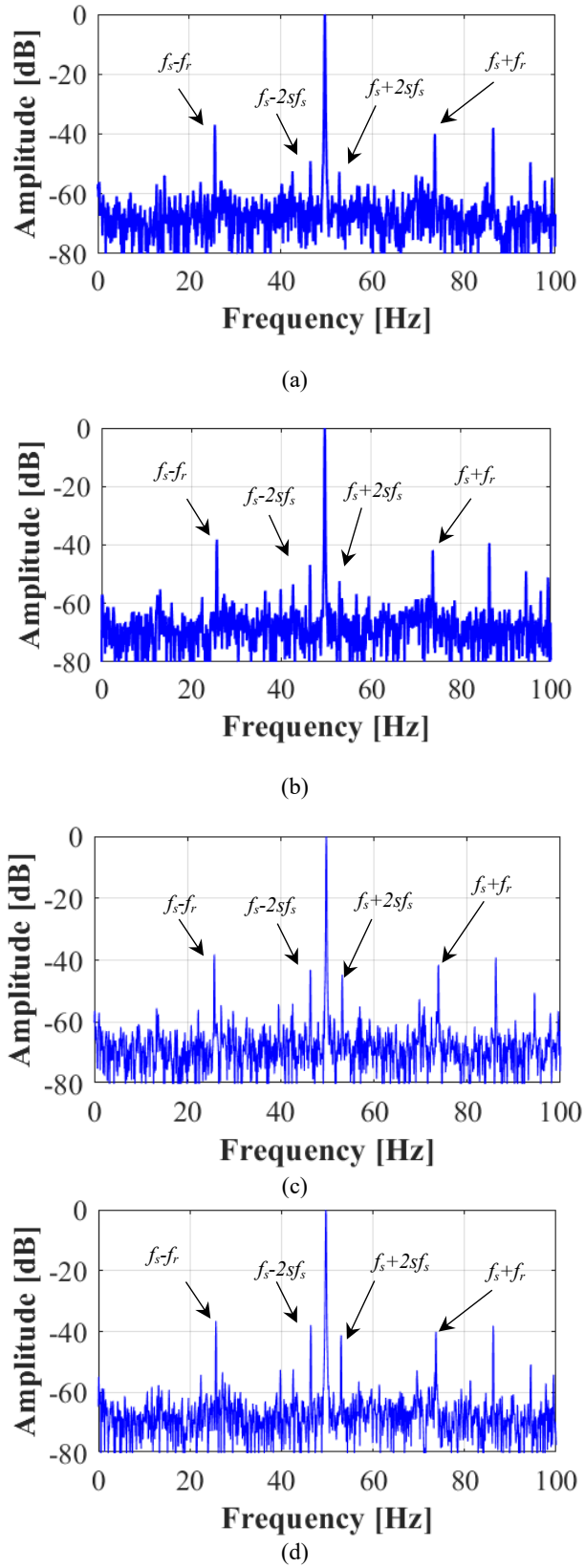


Fig. 6. FFT of the coil sensor at 1440 rpm a) Healthy b) One ohm c) 3 ohms d) 5 ohms.

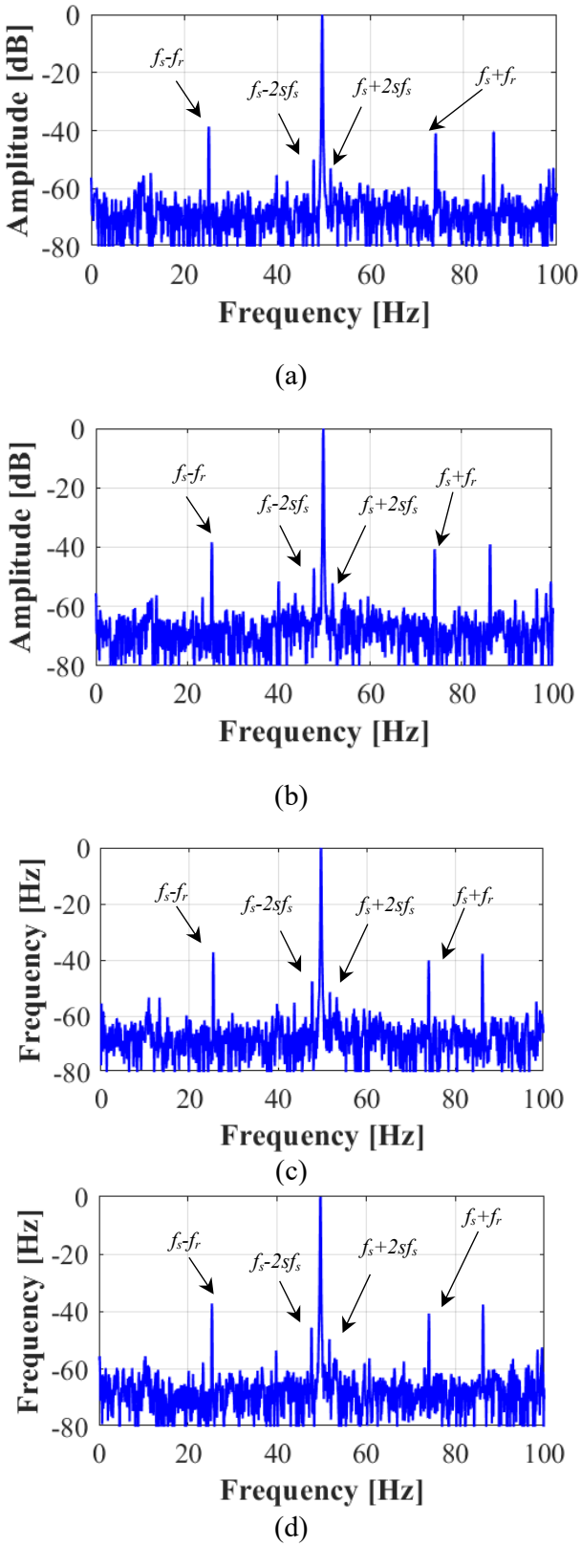


Fig. 7. FFT of the coil sensor at 1460 rpm a) Healthy b) One ohm c) 3 ohms d) 5 ohms.

ity analysis summarized in Table 3, the TKEO offers remarkably low computational complexity, rendering it highly suitable for real-time condition monitoring applications where processing power and latency constraints

TABLE 2. Fault Indices of the flux signal measured by the coil sensor (Values in dB normalized to the fundamental component: $20\log_{10}(A_{fault}/A_{fundamental})$).

Fault Indices	Speed	Healthy	1 ohm	3 ohm	5 ohm
$f_s - f_r$	1460	−38.61	−38.34	−37.27	−37.1
$f_s + f_r$		−40.91	−40.62	−40.1	−40.59
$f_s - 2sf_s$		−50.23	−47.06	−48.02	−45.69
$f_s + 2sf_s$		−52.97	−52.14	−51.44	−49.51
$f_s - f_r$	1440	−36.92	−38.16	−38.13	−36.56
$f_s + f_r$		−39.99	−41.86	−41.52	−40.11
$f_s - 2sf_s$		−49.07	−46.76	−43.13	−37.86
$f_s + 2sf_s$		−52.61	−52.34	−44.69	−41.25
$f_s - f_r$	1420	−37.06	−40.78	−36.65	−36.97
$f_s + f_r$		−41.88	−40.88	−40.62	−40.97
$f_s - 2sf_s$		−47.23	−41.71	−37.49	−34.83
$f_s + 2sf_s$		−50.48	−47.73	−39.16	−36.06

TABLE 3. Computational complexity and execution time of demodulation methods.

Method	Time (s)
TKEO	0.0049
ROAT	0.0161
FDEO	0.0374

are critical. As illustrated in Figs. 8–10, along with the quantitative results summarized in Table 3, the TKEO effectively isolates and highlights the fault characteristic frequency at $2sf_s$ under low-slip conditions, encompassing healthy operation as well as fault severities corresponding to 1 Ω, 3 Ω, and 5 Ω external rotor resistances. Notably, the TKEO consistently delivers superior diagnostic clarity across all tested conditions while maintaining the lowest computational complexity compared with ROAT and FDEO.

A key practical advantage of the TKEO method is its computational efficiency. As summarized in Table 3, the TKEO requires only 0.0049 s (4.9 ms), compared with 0.0161 s for ROAT and 0.0374 s for FDEO. These execution times were obtained on an entry-level Intel Celeron N4000 CPU at 1.10 GHz, a low-power processor representative of the hardware used in practical edge monitoring systems. The 4.9 ms execution time on such modest hardware confirms that the proposed method is sufficiently lightweight for real-time implementation on low-cost DSPs and microcontrollers. Since each TKEO computation requires only three consecutive samples, as shown in (10), it also imposes minimal memory requirements, making it suitable for embedded edge-computing platforms. As presented in Table 4, the application of the TKEO method reveals that the $2sf_s$ component exhibits strong sensitivity to both the occurrence and progression of the rotor fault. Specifically, the introduction of external resistance, followed by its incremental increase, results in a consistent and monotonic rise in the amplitude of this fault indicator across the entire speed range from 1420 rpm to 1460 rpm.

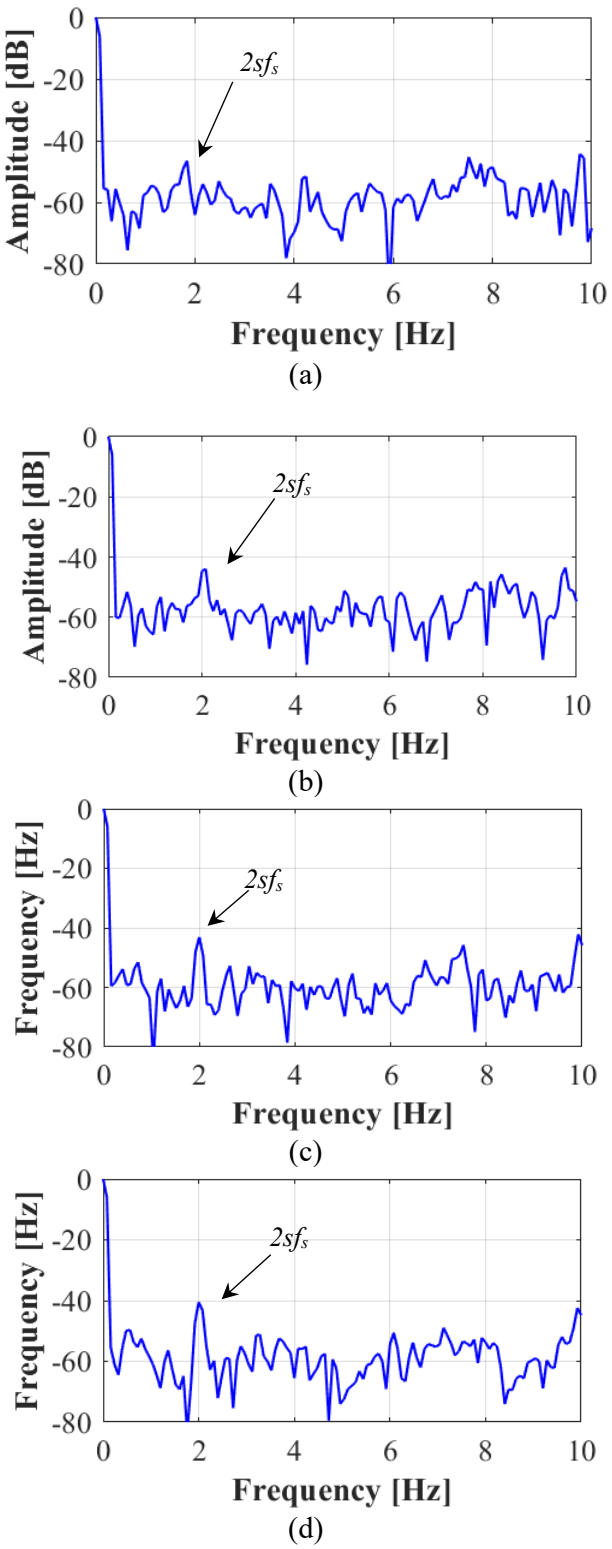


Fig. 8. FFT of the coil sensor at 1420 rpm a) Healthy b) One ohm c) 3 ohms d) 5 ohms.

V Conclusion

This study investigated the detection of rotor unbalance in a wound-rotor induction motor using stray flux signals at 1420, 1440, and 1460 rpm. Although FFT-based analysis successfully extracted the $f_s \pm 2sf_s$ fault indices, it required monitoring multiple indicators, some of which—such as $f_s \pm f_r$—are inherently unreliable for

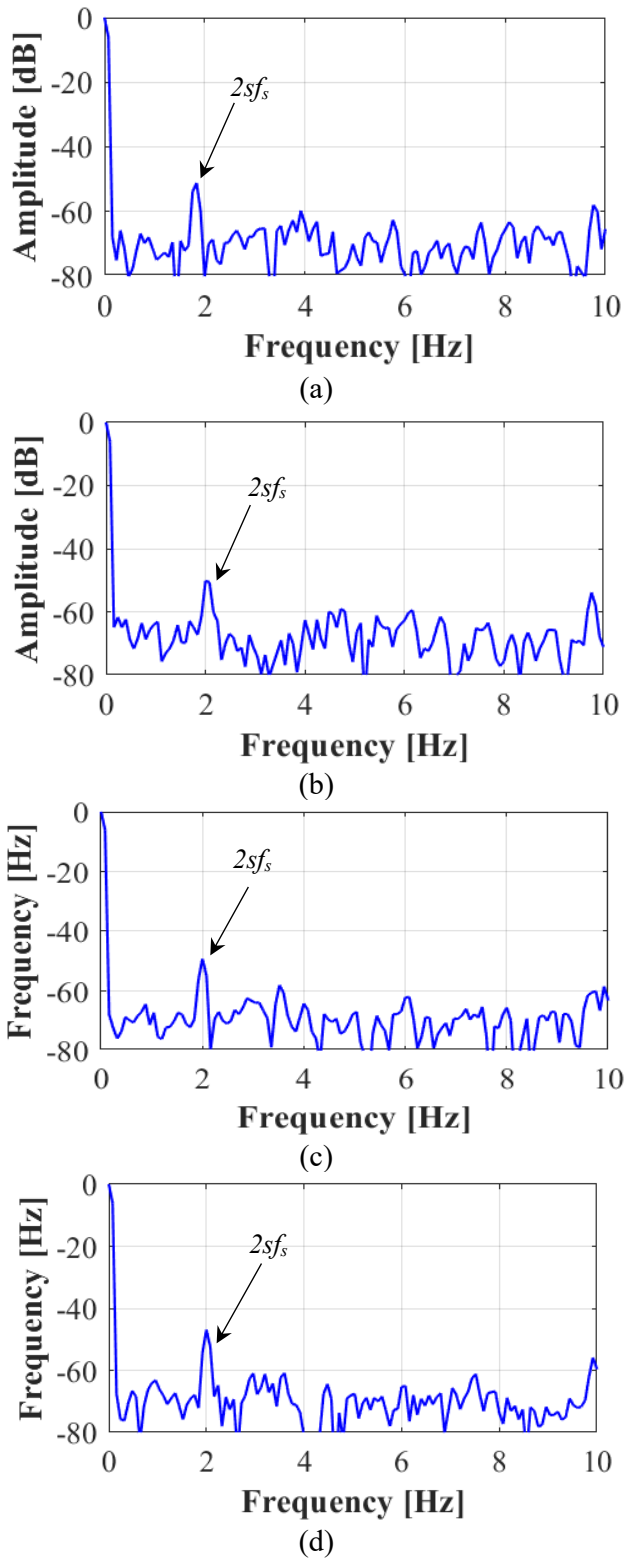


Fig. 9. FFT of the coil sensor at 1440 rpm a) Healthy b) One ohm c) 3 ohms d) 5 ohms.

rotor fault diagnosis. To address this limitation, the TKEO was applied to the stray flux signal, effectively suppressing the 50 Hz supply-frequency interference and consolidating all fault information into a single index at $2sf_s$, while maintaining very low computational complexity. The experimental results confirmed that the $2sf_s$ component exhibited a clear, monotonic increase with fault severity across all tested speeds, particularly at 1460 rpm. The proposed TKEO-based approach therefore offers a robust, efficient, and practical solution for real-time rotor fault diagnosis.

TABLE 4. Amplitude of fault characteristic frequency ($2sf_s$) dB in different load and unbalance fault sensor (Values in dB normalized to the fundamental component: $20\log_{10}(A_{fault}/A_{fundamental})$).

Speed (RPM)	Healthy	1-Ohm	3-Ohm	5-Ohm
1460	−46.54	−43.98	−43.14	−40.51
1440	−49.14	−44.49	−37.31	−34.98
1420	−43.68	−40.17	−32.65	−31.1

References

[1] Antonino-Daviu, J.A., Quijano-Lopez, A., Rubbiolo, M., Climente-Alarcon, V., Advanced analysis of motor currents for the diagnosis of the rotor condition in electric motors operating in mining facilities, *IEEE Trans. Ind. Appl.*, vol. 54, no. 4, pp. 3934–3942, 2018.

[2] Shin, S., Kim, J., Lee, S.B., Lim, C., Wiedenbrug, E.J., Evaluation of the influence of rotor magnetic anisotropy on condition monitoring of two-pole induction motors, *IEEE Trans. Ind. Appl.*, vol. 51, no. 4, pp. 2951–2959, 2015.

[3] Halder, S., Bhat, S., Zychma, D., Sowa, P., Broken rotor bar fault diagnosis techniques based on motor current signature analysis for induction motor—A review, *Energies*, vol. 15, no. 22, p. 8569, 2022.

[4] Hajnayeb, S., Marzebali, M.H., Abolghasemi, V., Faiz, J., Broken Rotor Bar Fault Detection of Induction Machine Based on Rectified Orthogonal Axes of Stator Current, *IEEE Transactions on Instrumentation and Measurement*, vol. 73, pp. 1–13, 2024, Art no. 3539913.

[5] Hajnaeb, S., Seyyed Barzegar, S.M., Hoseintabar Marzebali, M., Keighobadi, J., Diagnosis of Broken Rotor Bars in Induction Machines Using a Current Signature-Based Adaptive Extended Kalman Filter, In *Proceedings of the 2025 5th International Conference on Electrical Machines and Drives (ICEMD)*, pp. 1–6, 2025.

[6] Mazaheri-Tehrani, E., Faiz, J., Airgap and stray magnetic flux monitoring techniques for fault diagnosis of electrical machines: An overview, *IET Electric Power Applications*, 2021.

[7] Verma, S.P., Singal, R.K., Williams, K., Vibration behaviour of stators of electrical machines, Part I: Theoretical study, *Journal of Sound and Vibration*, vol. 115, no. 1, pp. 1–12, 1987.

[8] Li, L., Guo, J., Tan, Y., Zhou, Z., Recent advances and tendency in fiber Bragg grating-based vibration sensor: A review, *IEEE Sensors Journal*, vol. 20, no. 20, pp. 12074–12087, 2020.

[9] Bouchikhi, E., Choqueuse, V., Benbouzid, M., Current frequency spectral subtraction and its contribution to induction machines' bearings condition monitoring, *IEEE Transactions on Energy Conversion*, vol. 28, no. 1, pp. 135–144, 2013.

[10] Puche-Panadero, R., Martinez-Roman, J., Sapena-Bano, A., Burriel-Valencia, J., Diagnosis of rotor asymmetries faults in induction machines using the rectified stator current, *IEEE Transactions on Energy Conversion*, vol. 35,

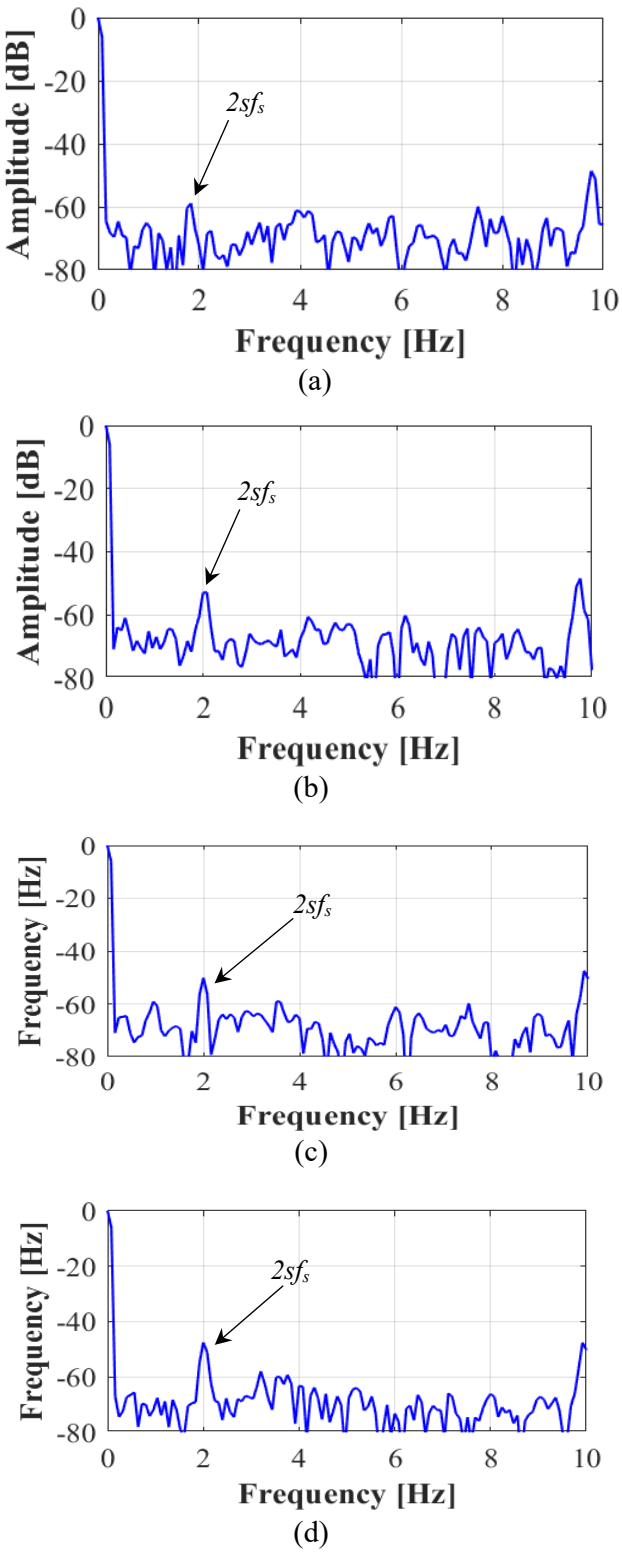


Fig. 10. FFT of the coil sensor at 1460 rpm a) Healthy b) One ohm c) 3 ohms d) 5 ohms.

no. 1, pp. 213–221, 2019.

[11] Hajnayeb, S., Amerian, F., Marzebali, M.H., Abolghasemi, V., Seyyedbarzegar, S.M., Broken Rotor Bar Fault Detection in Induction Machines Based on Rectified Three-Phase Stator Currents, In: *Proceedings of the 10th International Conference on Signal Processing and Intelligent Systems (ICSPIS)*, pp. 22–26, 2024.

[12] Bazghandi, R., Marzebali, M.H., Abolghasemi, V., Asymmetrical fault detection in induction motors through elimination of load torque oscillations effects in the slight speed variations and steady-state conditions, *IEEE Journal of Emerging and Selected Topics in Industrial Electronics*, vol. 4, no. 3, pp. 725–733, 2022.

[13] Henao, H., Demian, C., Capolino, G.A., A frequency-domain detection of stator winding faults in induction machines using an external flux sensor, *IEEE Transactions on Industry Applications*, vol. 39, no. 5, pp. 1272–1279, 2003.

[14] Pineda-Sanchez, M., *et al.*, Application of the Teager–Kaiser energy operator to the fault diagnosis of induction motors, *IEEE Transactions on Energy Conversion*, vol. 28, no. 4, 2013.

[15] Pusca, R., Romary, R., Advances in diagnosis of electrical machines through external magnetic field, In: *Proceedings of the 2015 7th International Conference on Electronics, Computers and Artificial Intelligence (ECAI)*, pp. P-5, 2015.

[16] Pusca, R., Romary, R., Ceban, A., Brudny, J.F., An online universal diagnosis procedure using two external flux sensors applied to the AC electrical rotating machines, *Sensors*, vol. 10, no. 11, pp. 10448–10466, 2010.

[17] Liang, X., Ali, M.Z., Zhang, H., Induction Motors Fault Diagnosis Using Finite Element Method: A Review, *IEEE Transactions on Industry Applications*, vol. 56, no. 2, pp. 1205–1217, 2020.

[18] Lamim Filho, P.C.M., Rabelo, L.M., Batista, F.B., Araújo, A.C., Orbit analysis from a stray flux full spectrum for induction machine fault detection, *IEEE Sensors Journal*, vol. 21, no. 14, pp. 16152–16161, 2021.

[19] Gyftakis, K.N., Panagiotou, P.A., Lee, S.B., Generation of mechanical frequency related harmonics in the stray flux spectra of induction motors suffering from rotor electrical faults, *IEEE Transactions on Industry Applications*, vol. 56, no. 5, pp. 4796–4803, 2020.